Atmospheric effect on microwave polarimetric passive remote sensing of ocean surfaces

Chen-Pang Yeang

Research Laboratory of Electronics, Massachusetts Institute of Technology

Simon H. Yueh

Jet Propulsion Laboratory, California Institute of Technology

Kung-Hau Ding, Jin Au Kong

Research Laboratory of Electronics, Massachusetts Institute of Technology

Abstract

A theoretical emission model of combined ocean surface and atmosphere is presented to predict the microwave emissivity of ocean. The modeled ocean surface is one-dimensional with a random rough profile. The electromagnetic scattering from the surface is calculated based on the Extended Boundary Condition method. Realizations of rough surfaces are created using Monte-Carlo simulations. The bistatic scattering coefficients are computed from the ensemble average. Millimeter-wave Propagation Model is used to evaluate the absorption of microwave radiation at all height levels in atmosphere. An expression for the observed brightness temperatures is derived by solving the radiative transfer equations. The radiative transfer model results show a good agreement with the measured data from 1995 NASA-JPL WINDRAD campaign. An approximate model is provided to estimate the atmospheric effect on the ocean brightness temperatures based on the overall atmospheric attenuation. The approximate model also compares well with the WINDRAD data. Further comparisons are made between the approximate formula and the radiative transfer results on the ratio of third Stokes parameter in atmosphere to the one in free space by varying the atmospheric conditions, surface roughness and radiation frequencies. The approximate formula shows its usefulness for the prediction of the ocean brightness temperatures.

polarimetry
ocean wind
radiometry

1. Introduction

In the microwave radiometry of ocean surface, observations of the emitting energy from ocean are used to characterize the physical state of the sea surface. The ocean thermal emission strongly depends on the surface roughness. Theoretical models for the polarimetric passive remote sensing of rough surfaces have been developed based on one-dimensional periodic dielectric surfaces [*Chuang and Kong*, 1982] [*Veysoglu*, 1991], one-dimensional random rough surfaces [*Yueh et al.*, 1994a], and two-dimensional random rough surfaces with a preferred corrugation direction [*Yueh et al.*, 1988]. Theoretical studies have indicated that the Stokes parameters are functions of the azimuth angle between the radiometer observation direction and the surface corrugation direction. This theoretical prediction has been verified by the controlled laboratory experiments [*Johnson et al.*, 1994] and the air-borne polarimetric measurement of ocean surfaces [*Yueh et al.*, 1995]. Several recent wind direction measurements [*Yueh et al.*, 1995], [*Yueh et al.*, 1994c] [*Yueh et al.*, 1994b] indicated that the angular dependence of Stokes parameters can be used to determine the surface corrugation direction, which is the direction of wind speed, and the amplitude of variation for Stokes parameters can be used to determine the surface roughness, which depends on the strength of wind speed. Thus, the measure of Stokes parameters are useful to invert the geometric characteristics of ocean surfaces.

The above theoretical studies model the ocean thermal emission in free space. However, the effects of atmosphere in the observed ocean brightness temperatures cannot be neglected. In *Pospelov* [1996], the atmospheric influence on sea-surface microwave emission is estimated by a simple radiative transfer process that treats the overall atmosphere as an uniform attenuative medium. The algorithm proposed in *Mukai et al.* [1997] computing the atmospheric correction for ocean color data concentrates on the effect of bistatic scattering from aerosols. These two works have neither come up with a comprehensive atmospheric model that includes both scattering from aerosols and absorption from air molecules at all height levels,

nor they have incorporated a rigorous electromagnetic surface scattering model to compute the interaction between the surface and the atmospheric radiation. *Kawata et al.* [1988] has developed a comprehensive radiative transfer model for the surface radiation propagating in a vertically heterogeneous atmosphere. But the albedoes and absorption coefficients at all height levels are not derived from the metereological data profiles. After simplification the only parameters that characterize the atmosphere are the overall optical depth and the constant aerosol density. Furthermore, in *Kawata et al.* [1988] the surface under atmosphere is modeled as a flat Lambertian plane with a horizontally non-uniform albedo distribution, which is less useful for the estimation of surface geometry compared with a rough-surface model. *West and Yueh* [1996] has incorporated a rigorous rough-surface scattering model and a comprehensive atmospheric model into the radiative transfer theory. The numerical results for brightness temperatures have fairly good agreement with the empirical data. However, in *West and Yueh* [1996] the sensitivity of brightness temperatures with respect to various conditions has not been thoroughly discussed. And the development of an atmospheric correction scheme on polarimetric radiometry on the basis of this framework remains to be exploited.

The objective of this paper is to investigate the atmospheric effects on the Stokes parameters of ocean surfaces from a rigorous electromagnetic surface scattering and comprehensive atmospheric model. It is also intended to exploit the possibility toward a scheme of atmospheric correction of ocean surface radiometry. In Section 2 we summarize the theory of polarimetric radiometry. The combined surface scattering and atmospheric model is presented in Section 3. The model consists of the scenario of a plane parallel, horizontally homogeneous atmosphere with an ocean rough surface at the bottom. The observed brightness temperatures of the ocean surface through atmosphere are calculated by solving the radiative transfer equations. The absorptive parameters and boundary conditions of the radiative transfer equations are obtained from the atmospheric model and surface scattering

model. The Millimeter-wave Propagation Model (MPM), which is applied as the atmospheric model, is briefly described. The surface scattering model is also presented. Unlike *West and Yueh* [1996] that adopts the approximate analytical approach, it is based on the Monte-Carlo simulation approach. The numerical results computed from this approach are compared with measured data from NASA-JPL's WINDRAD campaign. In Section 4 an approximate formula for calculating ocean thermal emission with atmospheric correction is presented. This approximate formula directly relates the observed ocean brightness temperatures with the overall atmospheric attenuation constants. By varying the simulation conditions, the results from approximate formula are compared with the results from the radiative transfer simulations. Section 5 is the summary.

2. Polarimetric Radiometry

In the polarimetric radiometry, the measured intensity of thermal emission is described by the Stokes vector **I**, which consists of four components I_h, I_v, U and V [*Tsang et al.*, 1985]:

$$\mathbf{I} = \begin{bmatrix} I_h \\ I_v \\ U \\ V \end{bmatrix} = \frac{1}{\eta} \begin{bmatrix} \langle E_h E_h^* \rangle \\ \langle E_v E_v^* \rangle \\ 2\,\mathrm{Re}\langle E_v E_h^* \rangle \\ 2\,\mathrm{Im}\langle E_v E_h^* \rangle \end{bmatrix} \tag{1}$$

In (1), E_h and E_v are the horizontal and vertical polarization components of the electric field, respectively, and $\eta = \sqrt{\mu_0/\epsilon_0}$ is the natural impedance. The four components I_h, I_v, U and V represent the respective radiation intensities of the horizontal and vertical polarizations, and the real and imaginary parts of the correlation between the horizontal and vertical polarizations.

The thermal radiation I_β emitted by an object under observation is proportional to its physical temperature T as in [*Tsang et al.*, 1985]:

$$I_\beta(\theta, \phi) = \frac{K}{\lambda^2} \cdot e_\beta(\theta, \phi) \cdot T, \tag{2}$$

where β refers to the polarization, K is Boltzmann constant, λ is the wavelength of the radiation, e_β is the emmisivity of the object, and (θ, ϕ) denotes the observation direction. The brightness temperature at polarization β, T_β, is defined as $T_\beta(\theta, \phi) = e_\beta(\theta, \phi)T$. In terms of the brightness temperatures, the Stokes vector $\mathbf{I}$ becomes

$$\mathbf{I} = \begin{bmatrix} I_h \\ I_v \\ U \\ V \end{bmatrix} = \frac{K}{\lambda^2} \begin{bmatrix} T_h \\ T_v \\ T_U \\ T_V \end{bmatrix} \tag{3}$$

It is shown in *Veysoglu* [1991] that the third and fourth Stokes parameters U and V may be related to the intensities at horizontal (I_h), vertical (I_v), 45° linear (I_p) and right-handed circular (I_r) polarizations:

$$U = I_h + I_v - 2I_p \tag{4}$$

$$V = I_h + I_v - 2I_r \tag{5}$$

respectively. The vector of brightness temperatures in (3) can be further expressed in terms of emissivities as

$$\begin{bmatrix} T_h \\ T_v \\ T_U \\ T_V \end{bmatrix} = T \begin{bmatrix} e_h \\ e_v \\ e_h + e_v - 2e_p \\ e_h + e_v - 2e_r \end{bmatrix} \tag{6}$$

Through the principles of energy conservation and reciprocity, Kirchhoff's law relates the emissivity to the reflectivity of the object [*Tsang et al.*, 1985]

$$e_\beta(\theta, \phi) = 1 - r_\beta(\theta, \phi) \tag{7}$$

where $r_\beta(\theta, \phi)$ is the reflectivity for the given incident polarization β and direction (θ, ϕ). For the ocean surface considered here, $r_\beta(\theta, \phi)$ can be evaluated by integrating bistatic scattering coefficients over all scattering angles in the upper hemisphere, and summing the results of both orthogonal scattering polarizations [*Tsang et al.*, 1985]. Once the bistatic scattering coefficients of the rough ocean surface are obtained, the fully polarimetric brightness temperatures are derived from (6) and (7).

3. Modeling of Ocean-Atmosphere Thermal Emission

The configuration of the passive remote sensing of ocean surface in atmosphere is illustrated in Figure 1. The radiometer is located at the upper sky ($z = 0$). The atmosphere beneath the sensor is modeled as a stack of plane-parallel and horizontally homogeneous layers. The lower half space ($z < -d$) is the ocean having a random rough surface profile, and with a complex permitivity ϵ_s, and a constant temperature T_s. The radiative transfer theory is used to compute the combined radiation from ocean surface and atmosphere. In order to formulate a set of precise radiative transfer equations, a surface scattering model that calculates the polarimetric ocean-surface emissivities, and an atmospheric model that quantitatively specifies the absorption, emission and scattering effects on the basis of metereological data, are required. After the atmospheric model and surface scattering model are combined through the radiative transfer equations, the brightness temperatures of the ocean surface observed through atmosphere can be computed.

Radiative Transfer Theory for the Ocean-atmosphere Emission

The propagation of thermal radiation in atmosphere can be described by the radiative transfer process. Within each layer, the radiation intensity is attenuated as well as enhanced due to absorption and emission by gaseous molecules and scattering from hydrosol particles. With the ocean-atmosphere configuration shown in Figure 1, the radiative transfer equations are applied to describe the propagation of radiation inside the atmosphere layer.

$$\cos\theta\frac{\partial}{\partial z}T_\alpha(\theta,\phi,z) = -\kappa_a(z)T_\alpha(\theta,\phi,z) + \kappa_a(z)T(z) \tag{8}$$

$$-\cos\theta\frac{\partial}{\partial z}T_\alpha(\pi-\theta,\phi,z) = -\kappa_a(z)T_\alpha(\pi-\theta,\phi,z) + \kappa_a(z)T(z) \tag{9}$$

with $0 \leq \theta \leq \pi/2$ and $0 \leq \phi \leq 2\pi$. $T_\alpha(\theta,\phi,z)$ represents the brightness temperature of polarization α in the direction (θ,ϕ) and at height z. Furthermore, $T_\alpha(\theta,\phi,z)$ describes the upgoing radiation intensity at height z, and $T_\alpha(\pi-\theta,\phi,z)$ the downgoing radiation

intensity. The parameter $\kappa_a(z)$ is the attenuation constant which is calculated from the Millimeter-wave Propagation Model and is independent of polarization. The atmospheric model MPM will be described later. $T(z)$ denotes the physical temperature at height z, and the product $\kappa_a(z)T(z)$ gives the emitted thermal radiation. Notice in (8) and (9) the term corresponding to the redistribution of radiation by the scattering of particles in atmosphere is neglected in this study because the frequency considered here is low (< 40 GHz) and in MPM the overall hydrosol scattering loss is included in a scalar propagation constant.

The boundary conditions at $z = 0$ and $z = -d$ are as follows:

$$T_\alpha(\pi - \theta, \phi, z = 0) = 0 \tag{10}$$

$$T_\alpha(\theta, \phi, z = -d) = T_s(1 - r_\alpha(\theta, \phi)) + \sum_\beta \int_{upper} d\Omega' \frac{1}{4\pi} \gamma_{\alpha\beta}(\theta, \phi; \theta', \phi') T_\beta(\pi - \theta', \phi', z = -d) \tag{11}$$

here the integral in (11) is over the upper hemisphere, $T_s = T(z = -d)$ is the physical temperature of ocean surface, and $\gamma_{\alpha\beta}(\theta, \phi; \theta', \phi')$ is the bistatic scattering coefficient of the rough surface from direction (θ', ϕ') and polarization β into direction (θ, ϕ) and polarization α, with $\{\alpha, \beta\} = \{v, h\}$. Boundary condition (10) assumes that the downgoing intensity at the upper sky is zero, i.e., the thermal radiation from the outer space is neglected. Boundary condition (11) states that the upgoing intensity at sea level is equal to the sum of the thermal radiation emitted from the rough surface and the scattered downgoing radiation emitted from the atmosphere. For a periodic rough surface, the second term on the right-hand side of (11) is the total sum of scattering energy corresponding to discretized floquet modes.

With the boundary conditions (10) and (11), the solution for the upgoing intensity in the direction (θ, ϕ) at $z = 0$ is [*Tsang et al.*, 1985]

$$T_\alpha(\theta, \phi, z = 0) = T_s(1 - r_\alpha(\theta, \phi)) \exp[-\int_{-d}^{0} dz'' \kappa_a(z'') \sec\theta]$$

$$+ \int_{-d}^{0} dz' \sec\theta \kappa_a(z') T(z') \exp[-\int_{z'}^{0} dz'' \kappa_a(z'') \sec\theta]$$

$$+ \exp[- \int_{-d}^{0} dz' \kappa_a(z') \sec \theta] \sum_{\beta=v,h} \int_{upper} d\Omega' \frac{1}{4\pi} \gamma_{\alpha\beta}(\theta, \phi; \theta', \phi')$$

$$\times \int_{-d}^{0} dz' \sec \theta' \kappa_a(z') T(z') \exp[- \int_{-d}^{z'} dz'' \kappa_a(z'') \sec \theta'] \tag{12}$$

The quantity $T_\alpha(\theta, \phi, z = 0)$ in (12) is the measured brightness temperature by the radiometer at the upper sky. The first term in (12) is the direct contribution of thermal emission from the ocean surface. The second term in (12) corresponds to the atmospheric emission that directly propagates toward the radiometer. The third term represents the atmospheric emission that is further scattered by the ocean surface before received by the radiometer. Each term experiences an attenuation, too.

The brightness temperature of ocean surfaces obtained from (12) has incorporated the contribution from the atmosphere. The reflectivity r_α and the bistatic scattering coefficient $\gamma_{\alpha\beta}$ of rough surfaces can be computed from a rough surface scattering model, and the attenuation constant κ_a can be specified by an atmospheric model. In this way, the combination of the surface scattering model and the atmospheric model is realized via (12).

Ocean Surface Scattering Model

In solving the radiative transfer equations the boundary condition at the ocean surface (11) requires a rough surface scattering model. The ocean surface scattering model consists of two parts: a model for the ocean surface spectrum, and a solution approach for the electromagnetic scattering field of the modeled ocean surface. In the polarimetric passive remote sensing, the ocean surface has been modeled as a stochastic process with a presumed ocean-like power spectrum [*Yueh et al.*, 1994a] [*Yueh et al.*, 1988] [*Yueh et al.*, 1994c]. Both analytical methods, such as Small Perturbation Method [*Yueh et al.*, 1988], and numerical methods, such as Method of Moment (MoM) [*Yueh et al.*, 1994a], have been applied to derive the mean scattering coefficients of the random rough surface. In the numerical approach, a Monte-Carlo simulation technique is employed to generate configurations of random rough

surfaces, solve the scattering problem for each surface realization, and then average over realizations [*Yueh et al.*, 1994a]. In this study, we use the Monte-Carlo simulation approach to derive the bistatic scattering coefficients of rough surfaces.

The ocean surface profile is assumed to be periodic and rough in only one dimension. As shown in Figure 1, the surface height is invariant along the y direction. The surface spectrum used by *Yueh et al.* [1994a] is adopted in this paper,

$$W(k_x, k_y) = q \sum_{n=1}^{10} k_x^{-3} \delta(k_x - nk_l) \delta(k_y) \tag{13}$$

where q is the amplitude of surface that adjusts the roughness, and all the frequency components in the surface power spectrum are multiples of a cutoff wavenumber k_l such that the surface has period $\lambda_l = 2\pi/k_l$.

Multiple realizations of random surface profiles are generated according to the power spectrum (13). For each realization of surface, the bistatic scattering coefficients are calculated by solving the integral equation based on the Extended Boundary Condition (EBC) technique. A detailed description for using EBC in solving rough surface scattering can be found in *Chuang and Kong* [1982]. The reason for using the Extended-Boundary-Condition approach rather than the traditional Method-of-Moment (MoM) approach is based on the concern for efficiency. As indicated in *Johnson* [1996], the EBC method performs faster than the MoM for non-steep rough surfaces.

The 1-D EBC program used in this paper is similar to the one in *Johnson* [1996]. It was executed on a DEC Alpha Machine (21164 Processor) with 256 megabytes of onboard RAM and 266 MHz speed. Energy conservation for this program is within 1%. The CPU time for computing the scattering coefficients corresponding to a specific wave incident direction and a specific rough surface profile is approximately 75 secconds. It was found that 10 realizations are adequate to make the Monte-carlo results converge.

Millimeter-wave Propagation Model (MPM)

The atmospheric model provides the quantitative effects of absorption, emission and scattering. To be precise, for each homogeneous layer the atmospheric model computes the numerical values of the effective attenuation constant and the bistatic phase matrix of radiation intensity from the metereological data within it. The atmospheric model used in this paper is the Millimeter-wave Propagation Model (MPM) [*Liebe*, 1985] [*Smith*, 1982]. The input data for MPM are temperature, barometric pressure and moisture. MPM calculates the effective attenuation and delay (i.e. the imaginary and real parts of the effective propagation constant) for a given radiation frequency from the input metereological data. The effects taken into account in this model include the absorption spectra of water and oxygen molecules, the dry-air absorption, and the scattering of EM waves due to hydrosol particles. The valid range of frequency is up to 1000 GHz. A detailed description for this model can be found in *Liebe* [1985]. Notice in MPM the hydrosol scattering effect is modeled in terms of, not a bistatic phase matrix, but an effective attenuation constant which is a scalar. If the effect of energy redistribution is taken into acount by modeling hydrosols as isotropic scatterers, then the source term in the radiative transfer equations (8) and (9), $\kappa_a(z)T(z)$, should be replaced by $\kappa_a(z)[\sigma_s(z)/\sigma_t(z)\bar{T}(z) + \sigma_a(z)/\sigma_t(z)T(z)]$, where $\bar{T}$ is the average of the brightness temperatures over directions and polarizations, and σ_t, σ_s, σ_a are the total, scattering, and absorption cross sections of a hydrosol particle [*Brussaard and Watson*, 1995]. For tiny water particles such as those in a cloud, the scattering albedo σ_s/σ_t is less than 0.5 for the whole millimeter wave frequency range [*Brussaard and Watson*, 1995]. Therefore the effect of energy redistribution is only comparable with the effect of hydrosol absorption in the worst case. In fact, for all the atmospheric profiles considered in this paper, the hydrosol absorption contributes only less than 2% of the overall attenuation. Hence the energy redistribution effect can be neglected.

With the Millimeter-wave propagation model and the data profiles of the atmospheric

temperature, pressure and moisture with respect to height level, the numerical values of the effective propagation constants of all the horizontal layers can be computed. Figure 2 illustrates the numerical results of accumulated attenuation and delay of all the horizontal layers versus frequency. The metereological data are from US Standard Atmosphere 1976 [*NOAA et al.*, 1976]. Four nadir angles (30°, 40°, 50° and 60°) are considered. The peaks in the absorption diagram correspond to the resonant frequencies of water and oxygen molecules. It is observed that, consistent with intuition, the higher the nadir angle is, the larger the absorption is.

Comparison of Model and Measurement

A series of polarimetric passive remote sensing experiments of ocean has been conducted by Jet Propulsion Laboratory (JPL), details of experimental observations are given in the literature [*Yueh et al.*, 1995]. The data set presented in this section for model comparison are NASA-JPL K-band polarimetric WINDRAD data [*Yueh et al.*, 1995]. The WINDRAD data were measured by the radiometer operating at 19.35 GHz installed on an aircraft that flew at 27000 to 30000 ft above the sea level. The measurement was carried out around the outer coast of north California, in early November, 1993. Four components were measured: horizontal brightness temperature T_h, vertical brightness temperature T_v, real part of the correlation between two orthogonal polarizations T_U, and the difference between two orthogonal polarizations $T_Q = T_h - T_v$.

The radiative transfer model described previously is used to simulate the ocean-atmosphere thermal emission. The Monte-Carlo technique is applied to treat the scattering from rough ocean surface and to derive the statistical average of polarimetric brightness temperatures. The Monte-Carlo procedures are as follows. First, realizations of one-dimensional periodic random rough surfaces are created based on the spectrum described in (13). Given an observation direction, the surface-scattering problem is solved by using the EBC method. All the

scattering coefficients at the upper hemisphere for each ocean-atmosphere configuration are calculated. Then, the surface bistatic scattering coefficients and the absorption coefficients from MPM are used to compute the polarimetric brightness temperatures via (12). This procedure is repeated for every ocean-atmosphere realization, and the results for brightness temperatures are obtained by averaging over configurations. Ten ocean-surface configurations are actually used to perform the Monte-Carlo averaging. The other parameters used in simulations are as follows. The radiation frequency is 19.35 GHz. The correlation length λ_l of the ocean-like surface is 6.28 cm, and the rms height is 1 mm. The ocean temperature is assumed to be 12°C, and of salinity 35 ppt. The permitivity of the ocean is $\epsilon_s = (28.59 + i36.89)\epsilon_0$ which is obtained from the empirical formula given by *Klein and Swift* [1977]. Sixteen azimuth angles between 0° and 360° are chosen. The metereological data used in simulations is based on US Standard Atmosphere 1976 [*NOAA et al.*, 1976]. The thickness of atmosphere is 8300 m. The humidities at height levels of atmosphere are modified to be consistent with the moisture data (recorded in *Direction of the Chief of Naval Operations* [1956]) of north California coast in November.

To investigate the atmospheric effects on the polarimetric ocean brightness temperatures, both cases of thermal emission from ocean with and without atmosphere are studied. For the case of without atmosphere, the medium between the ocean surface and the radiometer is free space, we only need to integrate the scattering coefficients over the upper hemisphere in (12) to obtain the brightness temperatures. Figure 3 and 4 show the comparison between the model and the measured brightness temperatures from WINDRAD data for observation directions of 30° and 40°, respectively. In both diagrams, the horizontal axis denotes the azimuth angle with respect to the surface corrugated direction, and the vertical axis denotes the brightness temperature. Measurement data show that the brightness temperatures T_h, T_v and T_U are all (approximately) simple harmonic functions of azimuth angle ϕ. This feature is also presented in the simulations no matter the atmospheric effect is incorporated

or not. However, the simulated T_h and T_v without the atmospheric effect are 15°K to 25°K less than the experimental data, When the atmospheric effect is included, the values of T_h and T_v agree reasonably well with WINDRAD data at both nadir angles. As shown in Figure 3(c) and 4(c), the values for the third Stokes parameter T_U both with and without the atmospheric effect match well with the WINDRAD data, but the incorporation of the atmosphere makes T_U attenuated slightly.

4. Approximate Radiation Model

The theoretical model of (12) requires the metereological information at all atmospheric height levels. However, in most practical cases, only the temporal and spatial average for these atmospheric quantities, such as US Standard Atmosphere 1976, are available. The exact metereological information about the specific atmosphere where the radiometric measurements are carried out is usually lacking. On the other hand, certain atmospheric quantities corresponding to the overall effect of the specific atmosphere, such as attenuation, could be obtained concurrently by carrying out proper measurements along with radiometry. In this section, we present an approximate model for the ocean surface brightness temperature which includes the atmospheric contribution but requires only the specification of the overall atmospheric attenuation. The validity range for this approximate model is also investigated by comparing with the numerical results from the model described in Section 3.

The approximate model is the first step toward an atmospheric correction scheme for the ocean radiometry data. They are derived based on two assumptions. First, we assume that the ocean surface roughness is small, thus most of the overall scattering energy will be concentrated at the specular direction. Second, the air temperature is assumed to be a constant over the region which contributes most of the atmospheric attenuation. Figure 5 illustrates the profiles of atmospheric attenuation constant $\kappa_a(z)$ and temperature $T(z)$ for the US Standard Atmosphere 1976. It shows that the attenuation constant drops much

faster than temperature. At $z = 3.65$ km, the atmospheric constant becomes one fourth of its peak value, while the air temperature decreases only one fifteenth of its peak value (about 20°K). Thus the second assumption is applicable.

Based on the first assumption, we replace the bistatic scattering coefficient $\gamma_{\alpha\beta}(\theta, \phi; \theta', \phi')/4\pi$ in (12) with $\delta_{\alpha\beta}\delta(\theta - \theta')\delta(\phi - \phi')$, r_α with $1 - e_\alpha$, and the term $\exp[-\int_{z'}^0 dz''\kappa_a(z'')\sec\theta]$ with the product of $\exp[-\int_{-d}^0 dz''\kappa_a(z'')\sec\theta]$ and $\exp[\int_{-d}^{z'} dz''\kappa_a(z'')\sec\theta]$. Thus equation (12) can be rewritten as

$$T_\alpha(\theta, \phi, z = 0) \approx T_s e_\alpha(\theta, \phi)\exp(-\kappa)$$

$$+[1 - e_\alpha(\theta, \phi)]\exp(-\kappa)\int_0^\kappa dx T(x)\exp(-x)$$

$$+\exp(-\kappa)\int_0^\kappa dx T(x)\exp(x) \tag{14}$$

where $\kappa = \int_{-d}^0 dz\kappa_a(z)\sec\theta$ is the overall attenuation, and the integration variable x is defined as

$$x(z) = \int_{-d}^z dz'\kappa_a(z')\sec\theta \tag{15}$$

Next, we apply the second assumption and let $T(x) = T(z = -d) \approx T_s$ for $0 \leq x \leq \kappa - \delta x$, where T_s is the temperature of ocean water, and δx is the amount of attenuation contributed from the region where T is a not constant. Since δx is small, the integrals in (14) can be approximated by

$$\int_0^\kappa dx T(x)\exp(x) \approx T_s[\exp(\kappa) - 1] \tag{16}$$

$$\int_0^\kappa dx T(x)\exp(-x) \approx T_s[1 - \exp(-\kappa)] \tag{17}$$

Substitute (16) and (17) into (15), we obtain a simple expression for the brightness temperatures:

$$T_\alpha(\theta, \phi, z = 0) \approx e_\alpha(\theta, \phi)T_s\exp(-2\kappa) + T_s(1 - \exp(-2\kappa)) \tag{18}$$

The first term on the right hand side of (18) is due to the ocean surface emission in free space, $e_\alpha T_s$, attenuated by the factor $\exp(-2\kappa)$. The second term, which does not depend

on the ocean surface characteristics, is contributed by the atmospheric thermal radiation. The approximate formula for T_U is

$$T_U \approx \exp(-2\kappa)(e_h + e_v - 2e_p)T_s$$

$$= \exp(-2\kappa)T_{U_{free}} \qquad (19)$$

where $T_{U_{free}}$ is the third Stokes parameter of the rough surface in free space. The surface-independent term of (18) has been canceled out in the derivation of T_U. Equation (18) approximates the measured T_U to be equal to the T_U of the ocean surface in free space times the square of overall atmospheric attenuation. Moreover, if we release the second assumption, that is, without the approximations of (16) and (17), the third Stokes parameter T_U is given as

$$T_U \approx \{\exp(-2\kappa) - \frac{1}{T_s}\exp(-\kappa)\int_0^\kappa dx[T(x) - T_s]\exp(-x)\}T_{U_{free}} \qquad (20)$$

Equations (18) and (19) provide simple expressions for the polarimetric ocean surface brightness temperatures with atmospheric corrections. However, they do not require complete metereological information, only the overall atmospheric attenuation factor $\exp(-\kappa)$ is needed. In addition, the ratio of T_U to $T_{U_{free}}$ is independent of the ocean surface characteristics. Figure 6 and 7 compares the brightness temperatures from the WINDRAD measurement and the results from the exact radiative transfer model in (12) and the approximate model in (18) and (19) at various azimuth angles ϕ and nadir angles $\theta = 30°$ and $40°$. All the parameter values used in numerical computations are identical to those used in Figure 3 and 4. Figure 6 and 7 indicate that, under the WINDRAD condition, the calculated polarimetric brightness temperatures from the approximate model are close to the results obtained from the exact model, and both values are consistent with the measured data.

In the remaining part of this section, we will investigate the sensitivity of the approximate radiation model by comparing the numerical results of T_U from the exact formula (12) with

the results from the approximate formula (19). The chosen simulation conditions are listed as follows:

- Atmospheres: US Standard Atmosphere 1976, average atmosphere at 15° and 60° latitude [Kunzi, 1986]

- Frequencies: 19.35 GHz, 22 GHz, 37 GHz

- Roughness: rms height 0.5 mm, 1 mm, 1.5 mm, 2.0 mm

Figure 8, 9 and 10 compare the ratios of T_U in atmosphere to T_U in free space from the exact radiative transfer model (12) with the ratios from the approximate formula (19). The nadir angle is varied from 0° to 70°. For each nadir angle θ, 17 ϕ angles evenly distributed from 0° to 360° are chosen. The default simulation condition is US Standard Atmosphere, surface rms height 1 mm, and 19.35 GHz. In each figure we vary only one condition from the default condition: atmospheric profile for Figure 8, surface roughness for Figure 9 and frequency for Figure 10. The asterisk symbols in these figures denote the values of $T_{U_{atmo}}/T_{U_{free}}$, where $T_{U_{atmo}}$ is T_U in atmosphere calculated from the approximate formula (19). The error bars denote the values of $T_{U_{atmo}}/T_{U_{free}}$, where $T_{U_{atmo}}$ is T_U in atmosphere calculated from from the exact radiative transfer model. Each error bar represents the region of standard deviation based on the statistics of 17 cases corresponding to different azimuth angles.

The results in the sub-diagrams of Figure 8, 9, and 10 show several significant common trends. First, the numerical values of $T_{U_{atmo}}/T_{U_{free}}$ from the approximate formula (18) are close to the values from the exact radiative transfer model (12), except at larger nadir angles (60° and 70°) or highly attenuated atmospheres (latitude 15°). Second, the ratios from the approximate formula decrease with increasing nadir angle. This trend is derived from the fact that at higher θ the overall attenuation constant $\exp(-2\kappa)$ is smaller. Third, the average of the numerical results for T_U ratios from the exact radiative transfer model is always

higher than the results predicted from the approximate formula. This phenomenon could be explained as follows. According to (20), the offset of the T_U ratio from the exact radiative transfer model to the T_U ratio from the approximate formula is $-\exp(-\kappa) \int_0^\kappa dx [T(x)/T_s - 1] \exp(-x)$. From Figure 5, the atmospheric temperature is monotonically decreasing with height. So $T(x)$ is always smaller or equal to surface temperature T_s. Hence the offset is always positive. Fourth, the offset of the T_U ratio increases with incident nadir angle as well as atmospheric attenuation. Both higher atmospheric attenuation and higher nadir angle render the overall attenuation constant smaller. Based on (20), we could show that, the smaller the overall attenuation constant is, the larger the offset of the T_U ratio becomes, in Appendix A. Fifth, unlike the prediction from the approximate formula (19), the T_U ratio from the exact radiative transfer model varies with azimuth angle ϕ. This variation is due to the existence of non-specular scattering energy, which is assumed to be vanished in deriving (19).

The three sub-diagrams in Figure 8 associate with different atmospheric and same surface scattering conditions. The air at lower latitude is more humid, therefore renders more serious absorption. From the figure it is clear that the one associated with the least absorptive atmosphere (60° latitude) has the smallest offset, and the one with the most absorptive atmosphere (15° latitude) has the largest offset, which is consistent with the explanation in Appendix A. The three sub-diagrams in Figure 9 associate with different surface scattering and same atmospheric conditions. Thus, at the same nadir angle the T_U ratios from the approximate formula are identical among different surface roughness. In general, except at higher nadir angles the T_U ratios from the exact radiative transfer model are not very different among different surface rms heights from 0.5 to 2 mm. This trend implies that at 19.35 GHz the patterns of energy distribution among the floquet modes are independent of the four chosen surface rms heights. The three sub-diagrams in Figure 10 associates with different frequencies. Both the atmospheric absorption and the surface scattering pattern

are varied by the change of frequency. Note that at 22 GHz, the one with the most significant atmospheric attenuation among the three chosen frequencies (c.f. Figure 2), the offset of the T_U ratio from the exact radiative transfer model to the T_U ratio from the approximate model is more irregular than the case of 15°-latitude atmosphere in Figure 8, even though their overall attenuation constants are about the same. This phenomenon indicates that when the radiation frequencies are different, it is inadequate to estimate the accuracy of the approximate formula with respect to the exact radiative transfer model merely in terms of the atmospheric absorption effect. The surface scattering effect and its combination with the atmospheric effect are also essential.

To sum up the observations, the results of T_U ratios from the approximate formula (19) have reasonable agreement with the exact radiative transfer model for lower nadir angles (up to 40°), drier atmospheres (60° latitude, US Standard Atmosphere), and radiation frequencies 19.35 GHz, 37 GHz, and less related to surface roughness (up to 2 mm rms height).

5. Summary

In this paper, we develop a model to evaluates the atmospheric effect on the millimeter-wave/microwave thermal emission from rough surfaces. This model is obtained by combining a surface scattering model with an atmospheric model. We use Monte-Carlo simulation to compute the scattering from an one-dimensional random rough surface with a fixed surface spectrum. We use Millimeter-wave Propagation Model with given metereological data profiles to calculate the atmospheric absorptions at all height levels. The combination of these two model is achieved via the radiative transfer theory. The Monte-Carlo simulation results generated by this model are then compared with the real data of brightness temperatures measured in the 1995 NASA-JPL WINDRAD campaign. At observation angles 30° and 40°, the simulation results for brightness temperatures agree reasonably with measured

data. Compared with the free-space condition, the T_h and T_v are about 15° to 25° higher, while the amplitude of the harmonic components of T_h, T_v, and T_U are more attenuated in atmosphere. We also propose an approximate model to estimate the atmospheric effect of brightness temperatures from the overall atmospheric attenuation. The ratio of the third Stokes parameter of the rough surface in atmosphere to the one in free space are computed from the exact radiative transfer model as well as the approximate formula. Different simulation conditions (varied atmospheres, surface roughness and frequencies) are applied to study the sensitivity of the approximate model. It is discovered that the results from the approximate model agree reasonably with those from the exact radiative transfer model at less attenuation conditions. The deviations of the results from the exact radiative transfer model with respect to the results from the approximate formula exhibit certain significant trends. These trends are explained by inspecting the assumptions from which the approximate model is derived.

Appendix A. Increasing Offset with Attenuation

In Section 4, the observation of Figure 8 to 10 indicates that the offset of the T_U ratio increases with the overall attenuation constant. To explain this observation, we consider a specific example. Suppose in case A, the height-dependent atmospheric attenuation is $\kappa_a(z)$ and the nadir angle is θ. Then from (20) its offset from the approximate formula, denoted as d_A, is

$$d_A = -\frac{1}{T_s} \exp[-\int_{-d}^{0} dz \kappa_a(z) \sec \theta] \int_{-d}^{0} dz \kappa_a(z) \sec \theta [T(z) - T_s] \exp[-\int_{-d}^{z} dz' \kappa_a(z') \sec \theta]$$

$$(A.1)$$

Equation (A.1) is obtained from converting the integral variable in (20) from x to z. Suppose in another case B, the product of the atmospheric attenuation and the second of the nadir angle is α times larger than the same product in case A, namely, $\alpha \kappa_a(z) \sec \theta$, where $\alpha > 1$.

Then the offset d_B is

$$d_B = -\frac{1}{T_s} \exp[-\alpha \int_{-d}^{0} dz \kappa_a(z) \sec \theta] \int_{-d}^{0} dz \alpha \kappa_a(z) \sec \theta [T(z) - T_s] \exp[-\alpha \int_{-d}^{z} dz' \kappa_a(z') \sec \theta]$$
$$(A.2)$$

From (A.1) and (A.2), the difference between d_A and d_B is

$$d_A - d_B = -\frac{1}{T_s} \exp[-\int_{-d}^{0} dz \kappa_a(z) \sec \theta] \int_{-d}^{0} dz \kappa_a(z) \sec \theta [T(z) - Ts] \exp[-\int_{-d}^{z} dz' \kappa_a(z') \sec \theta]$$

$$\times \{1 - \alpha \exp[-(\alpha - 1) \int_{-d}^{0} dz \kappa_a(z) \sec \theta - (\alpha - 1) \int_{-d}^{z} dz' \kappa_a(z') \sec \theta]\} \qquad (A.3)$$

Note the term within the bracket of the integrand of (A.3) satisfies the following inequality:

$$1 - \alpha \exp[-(\alpha - 1)\kappa] \leq 1 - \alpha \exp[-(\alpha - 1) \int_{-d}^{0} dz \kappa_a(z) \sec \theta - (\alpha - 1) \int_{-d}^{z} dz' \kappa_a(z') \sec \theta]$$

$$\leq 1 - \alpha \exp[-2(\alpha - 1)\kappa] \qquad (A.4)$$

for all z's, where $\kappa = \int_{-d}^{0} dz \kappa_a(z) \sec \theta$. In the cases considered in this paper, κ is small enough such that $\alpha \exp[-2(\alpha - 1)\kappa] \geq 1$. Therefore

$$1 - \alpha \exp[-(\alpha - 1) \int_{-d}^{0} dz \kappa(z) \sec \theta - (\alpha - 1) \int_{-d}^{z} dz' \kappa(z') \sec \theta] \leq 0 \qquad (A.5)$$

for all z's. Substitute (A.5) into (A.3), it can be shown that the difference $d_A - d_B \leq 0$. Furthermore, both d_A and d_B are positive. So the offset corresponding to a smaller $\kappa_a(z)$ or $\sec \theta$ (namely, a larger overall attenuation constant κ) is smaller than the offset corresponding to a larger $\kappa_a(z)$ or $\sec \theta$ (a smaller κ).

Acknowledgments

References

Brussaard, G., and P. A. Watson, *Atmospheric Modelling and Millimetre Wave Propagation*, Chapman and Hall, London, 1995.

Chuang, S. L., and J. A. Kong, Wave scattering from a periodic dielectric surface for a general angle of incidence, *Radio Science,* 17(3), 545 - 557, 1982.

Direction of the Chief of Naval Operations, *U.S. Navy Marine Climatic Atlas of the World, Vol II North Pacific Ocean,* NAVAER 50-1c-529, 1956.

Johnson, J. T., J. A. Kong, R. T. Shin, S. H. Yueh, S. V. Nghiem, and R. Kwok, Polarimetric thermal emission from rough ocean surfaces, *Journal of Electromagnetic Waves and Applications*, 8, 43 - 59, 1994.

Johnson, J. T., *Applications of Numerical Models for Rough Surface Scattering,* Ph. D. Thesis, Department of Electrical Engineering and Computer Science, Massachusetts Institute of Technology, 1996.

Kawata, Y., S. Ueno, and T. Kusaka, Radiometric correction for atmospheric and topographic effects on Landsat MSS images, *International Journal of Remote Sensing*, 9(4), 729 - 748, 1988.

Klein, L. A. and T. Swift, An improved model for the dielectric constant of sea water at microwave frequencies, *IEEE Transactions on Antenna and Propagation*, 25, 104-111, 1977.

Kunzi, K. F., *Report of Microwave Group on ITRA - Intercomparison Campaign Workshop,* University of Maryland, March 1986.

Liebe, H. J., An updated model for millimeter wave propagation in moist air, *Radio Science,* 20(5), 1069 - 1089, 1985.

Mukai, S., I. Sano, and K. Masuda, Algorithms for atmospheric correction for ocean color data", *Proceedings of IEEE International Geoscience and Remote Sensing Symposium*, 1896 - 1898, Singapore, 1997.

National Oceanic and Atmospheric Administration, National Aeronautics and Space Administration, United States Air Force, *U.S. Standard Atmosphere, 1976.*

Pospelov, M. N., The atmosphere influence on sea-surface polarized microwave emission, *Proceedings of IEEE International Geoscience and Remote Sensing Symposium*, 1135 - 1137, Lincoln, Nebraska, USA, 1996.

Smith, E., Centimeter and millimeter wave attenuation and brightness temperature due to atmospheric oxygen and water vapor, *Radio Science,* 17(6), 1455 - 1464, 1982.

Tsang, L., J. A. Kong, and R. T. Shih, *Theory of Microwave Remote Sensing*, John Wiley and Sons, New York, 1985.

Veysoglu, M. E., *Polarimetric Passive Remote Sensing of Periodic Surfaces and Anisotropic Media,* M. S. Thesis, Department of Electrical Engineering and Computer Science, Massachusetts Institute of Technology, 1991.

West, R. D., and S. H. Yueh, Atmospheric effects on the wind retrieval performance of satellite radiometers, *Proceedings of IEEE International Geoscience and Remote Sensing Symposium*, 1727 - 1729, Lincoln, Nebraska, USA, 1996.

Yueh, H. A., R. T. Shin, and J. A. Kong, Scattering of electromagnetic wave from a periodic surface with random roughness, *Journal of Applied Physics,* 64(4), 1657 - 1670, 1988.

Yueh, S. H., R. Kwok, F. K. Li, S. V. Nghiem, and W. J. Wilson, Polarimetric passive remote sensing of ocean wind vectors, *Radio Science,* 29(4), 799 - 814, 1994a.

Yueh, S. H., R. Kwok, and S. V. Nghiem, Polarimetric scattering and emission properties

of targets with reflection symmetry, *Radio Science,* 29(6), 1409 - 1420, 1994b.

Yueh, S. H., S. V. Nghiem, and R. K. Kwok, Comparison of a polarimetric scattering and emission model with ocean backscatter and brightness measurement, " *Proceedings of IEEE International Geoscience and Remote Sensing Symposium,* 258 - 260, Pasadena, California, USA, 1994c.

Yueh, S. H., W. J. Wilson, F. K. Li, S. V. Nghiem, and W. B. Ricketts, Polarimetric measurements of sea surface brightness temperatures using aircraft K-band radiometer, *IEEE Transactions on Geoscience and Remote Sensing,* 33(1), 85 - 92, 1995.

Figure Captions

Figure 1. Configuration of ocean-surface radiometry in atmosphere.

Figure 2. Overall atmospheric attenuation and delay from the MPM. The metereological data are based on US Standard Atmosphere 1976. The overall height is 30 km. The radiation frequency is up to 100 GHz. The values associated with four nadir angles are included: – 30°, . 40°, - - 50°, .-.- 60°.

Figure 3. Comparison of brightness temperatures of WINDRAD measurement with simulation results; nadir angle $\theta = 30°$; * WINDRAD data, + simulation w/o atmosphere, o simulation w/ atmosphere.

Figure 4. Comparison of brightness temperatures of WINDRAD measurement with simulation results; nadir angle $\theta = 40°$; * WINDRAD data, + simulation w/o atmosphere, o simulation w/ atmosphere.

Figure 5. The profiles of attenuation constant and air temperature in the US Standard Atmosphere 1976. The wave frequency is 19.35 GHz.

Figure 6. Comparison of brightness temperatures of WINDRAD measurement with the results from numerical RT model and approximate model. The nadir angle $\theta = 30°$, all the parameter values are the same as those in Figure 3; * WINDRAD data, + numerical model, o approximate model.

Figure 7. Comparison of brightness temperatures of WINDRAD measurement with the results from numerical RT model and approximate model. The nadir angle $\theta = 40°$, all the parameter values are the same as those in Figure 4; * WINDRAD data, + numerical model, o approximate model.

Figure 8. Comparison of T_U ratio from the exact RT model with the approximate formula.

Rough surface rms height is 1.0 mm. Frequency is 19.35 GHz. Three atmospheric profiles are considered: US Standard Atmosphere, 15° latitude, 60° latitude; error bar exact RT model, * approximate formula.

Figure 9. Comparison of T_U ratio from the exact RT model with the approximate formula. Rough surface rms height is 1.0 mm. Atmospheric profile is US Standard Atmosphere. Frequency is 19.35 GHz. Four rough surface rms height levels are considered: 0.5 mm, 1.0 mm, 1.5 mm, 2.0 mm; error bar exact RT model, * approximate formula.

Figure 10. Comparison of T_U ratio from the exact RT model with the approximate formula. Atmospheric profile is US Standard Atmosphere. Rough surface rms height is 1.0 mm. Three frequencies are considered: 19.35 GHz, 22 GHz, 37 GHz; error bar exact RT model, * approximate formula.
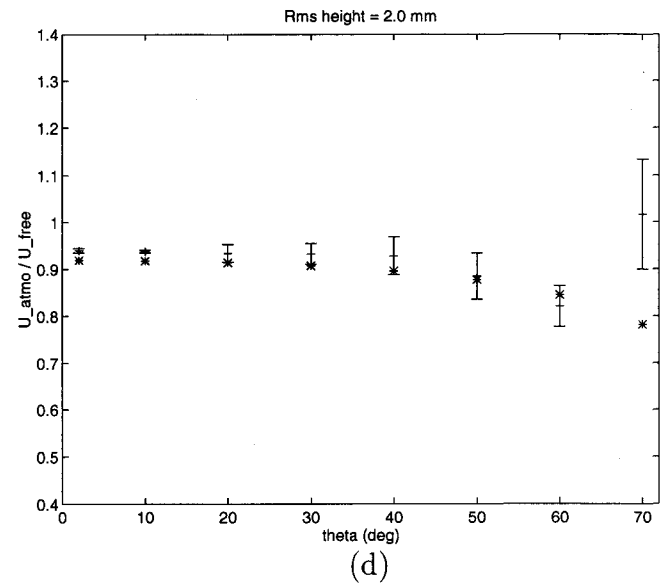
Yeang, Yueh, Ding, and Kong, Figure 1

Overall Atmospheric Absorption

Overall Atmospheric Delay

(a)

(b)
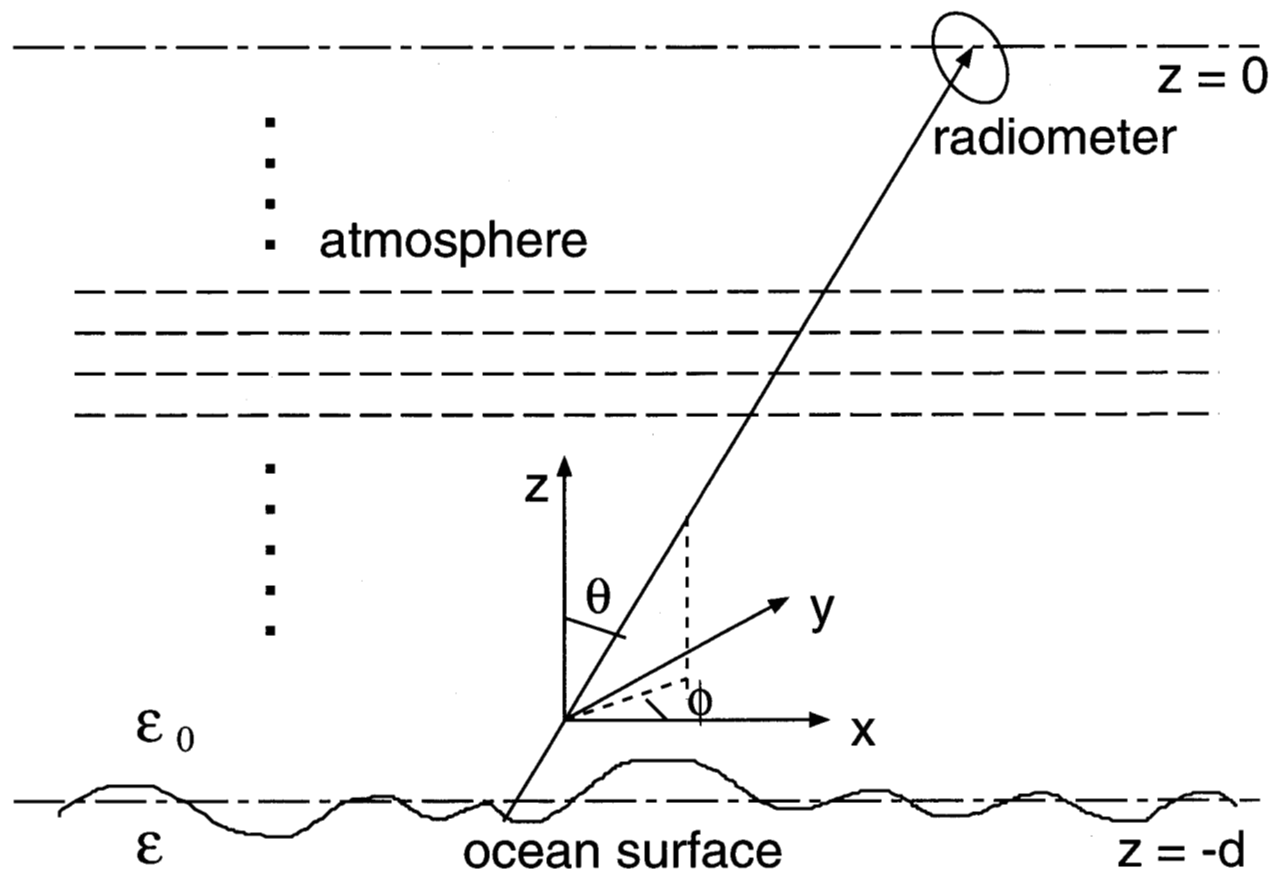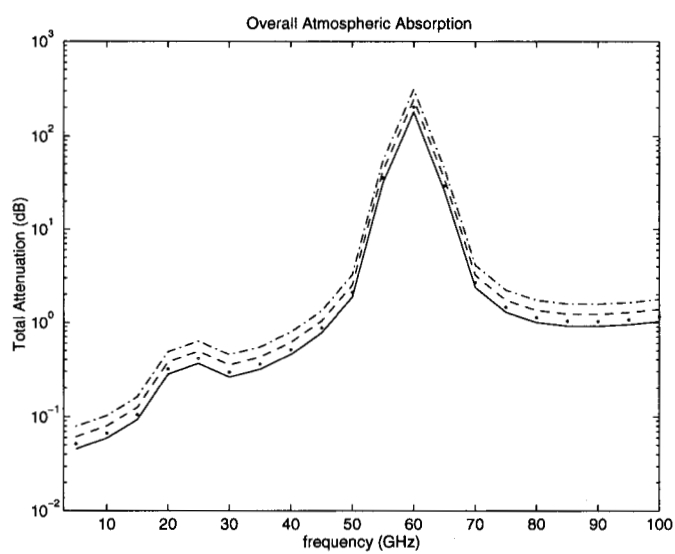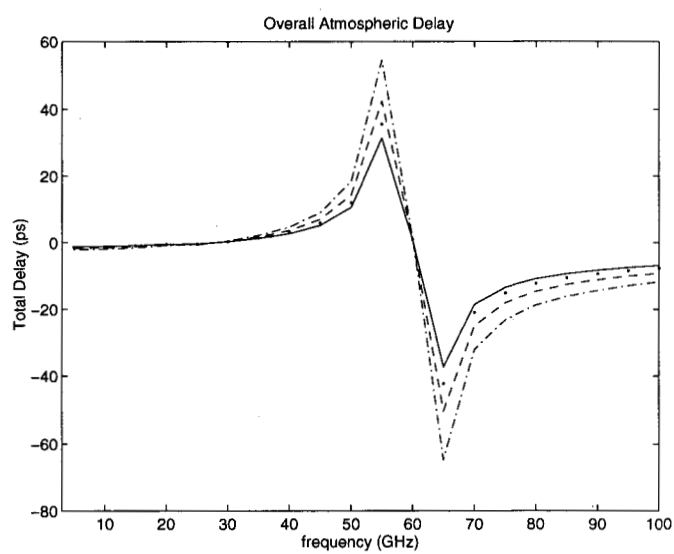
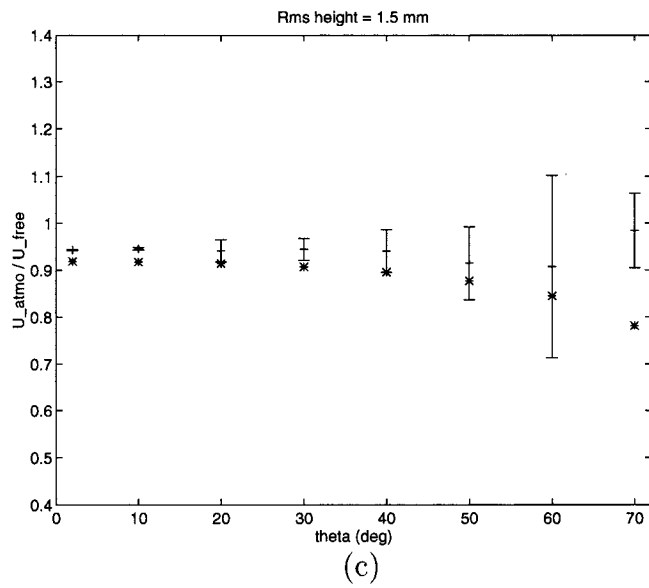Yeang, Yueh, Ding, and Kong, Figure 2

(a)

(b)

(c)
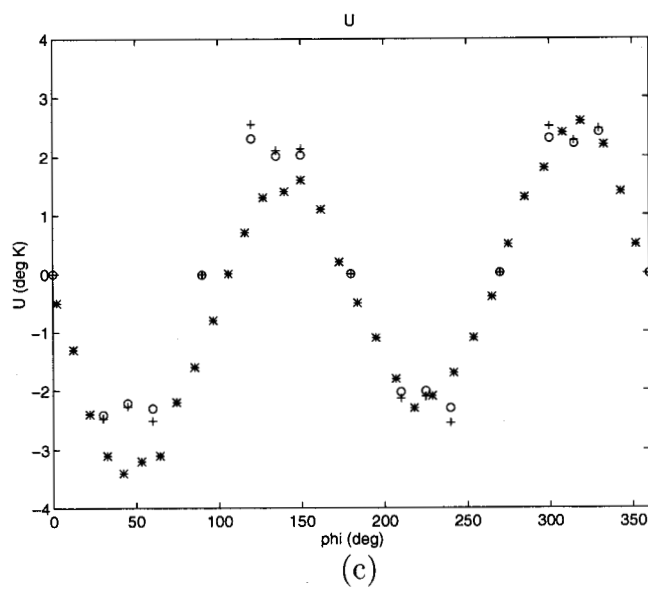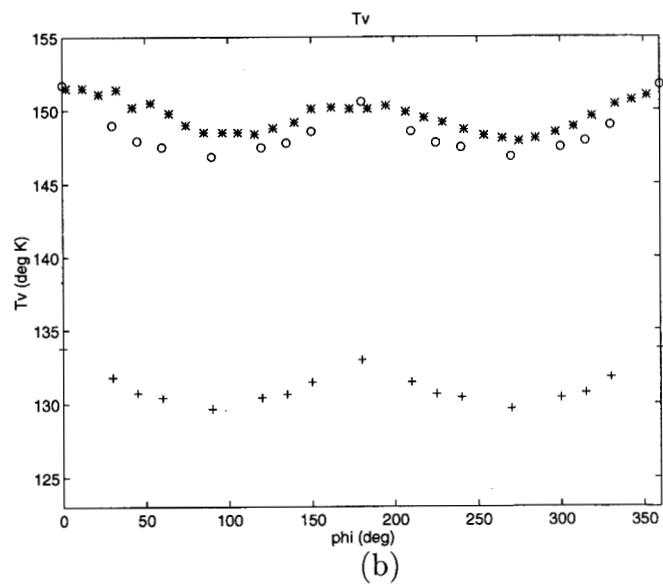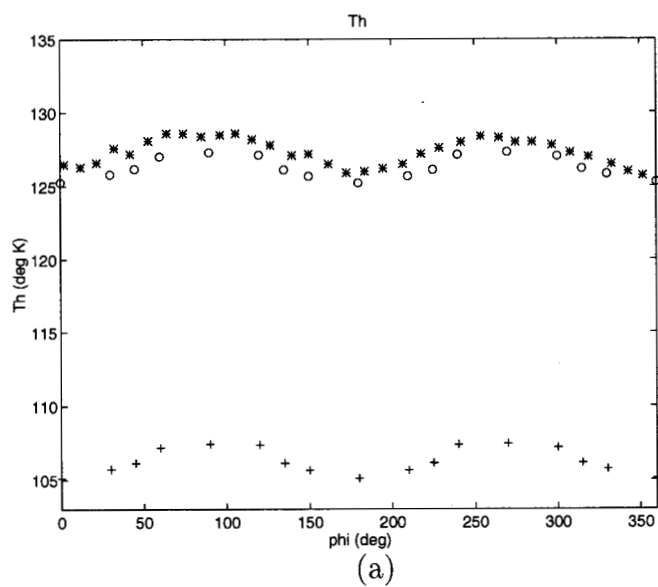
Yeang, Yueh, Ding, and Kong, Figure 3
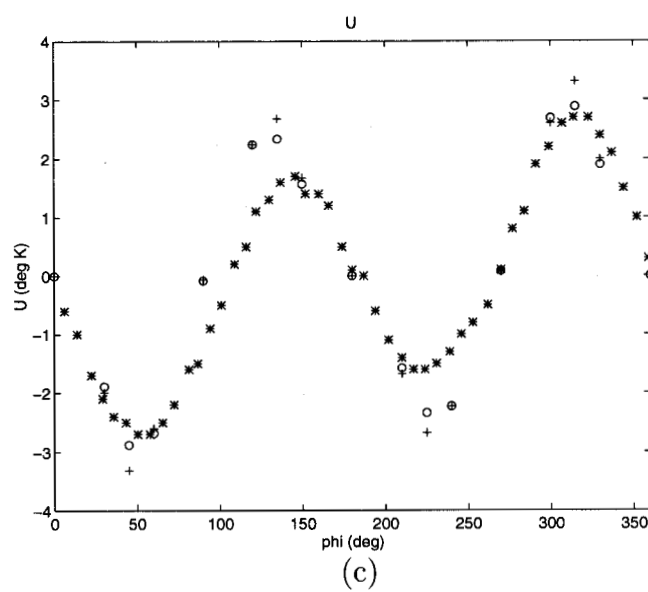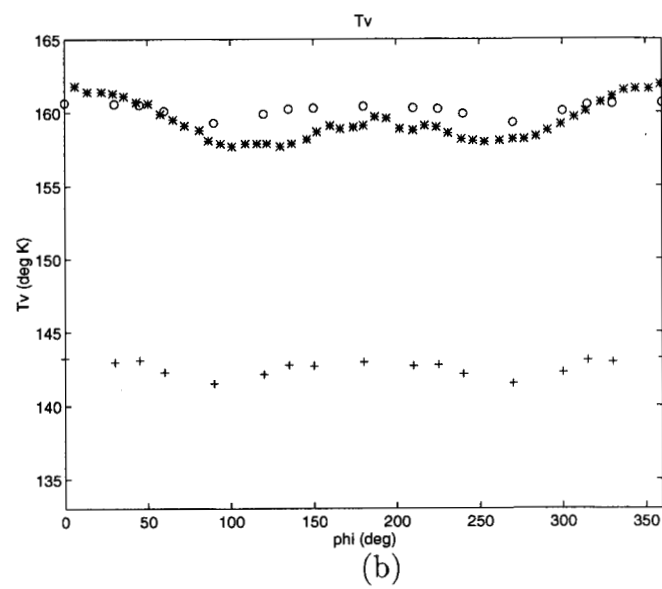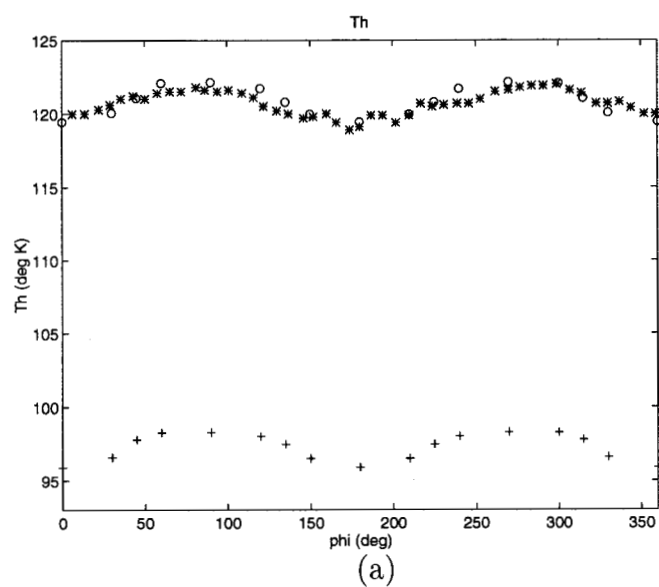
Yeang, Yueh, Ding, and Kong, Figure 4

(a)

(b)

Yeang, Yueh, Ding, and Kong, Figure 5

(a)

(b)

(c)
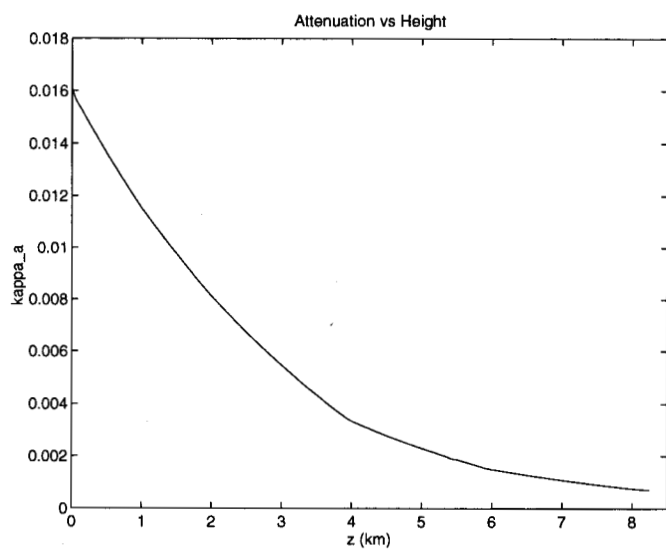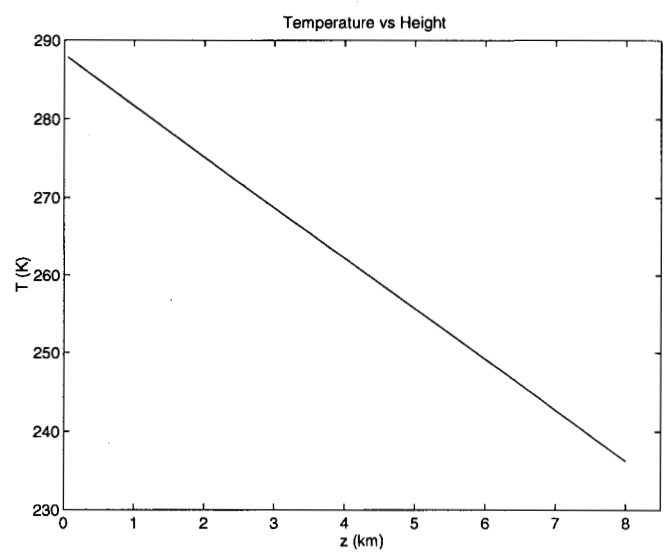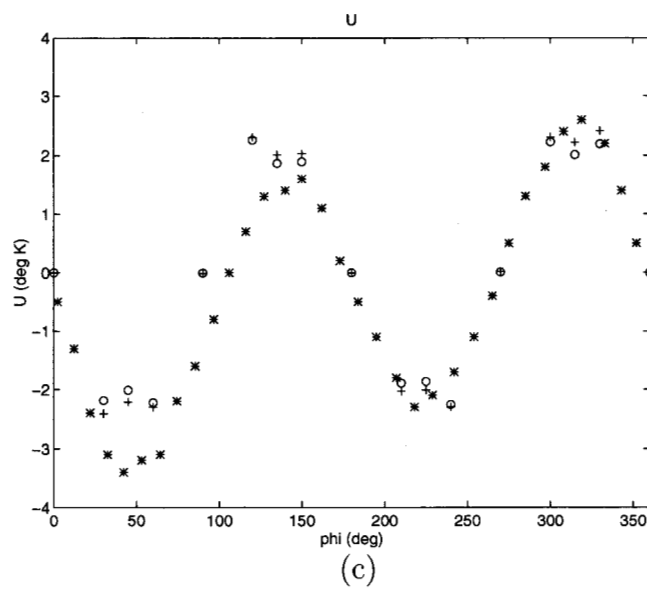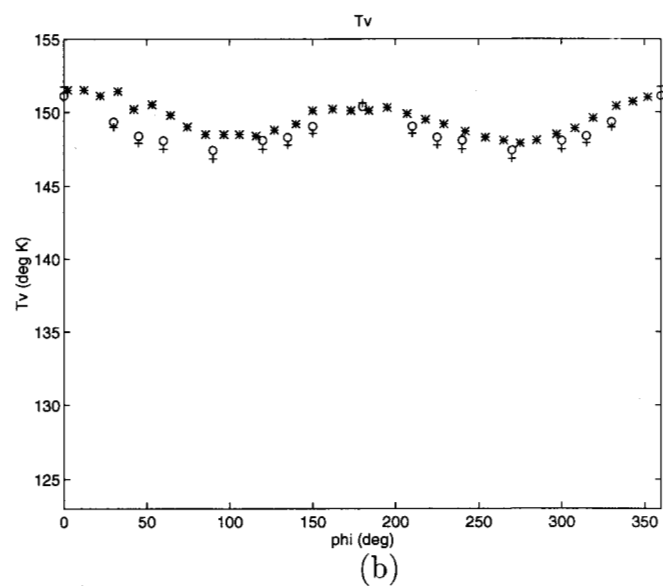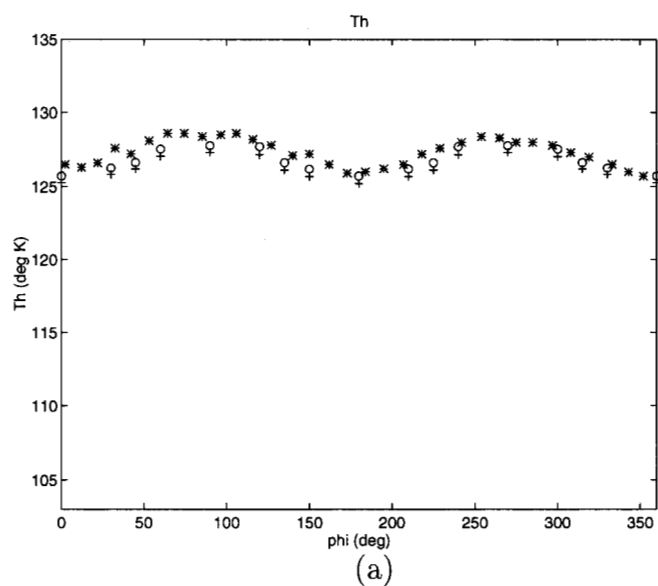
Yeang, Yueh, Ding, and Kong, Figure 6

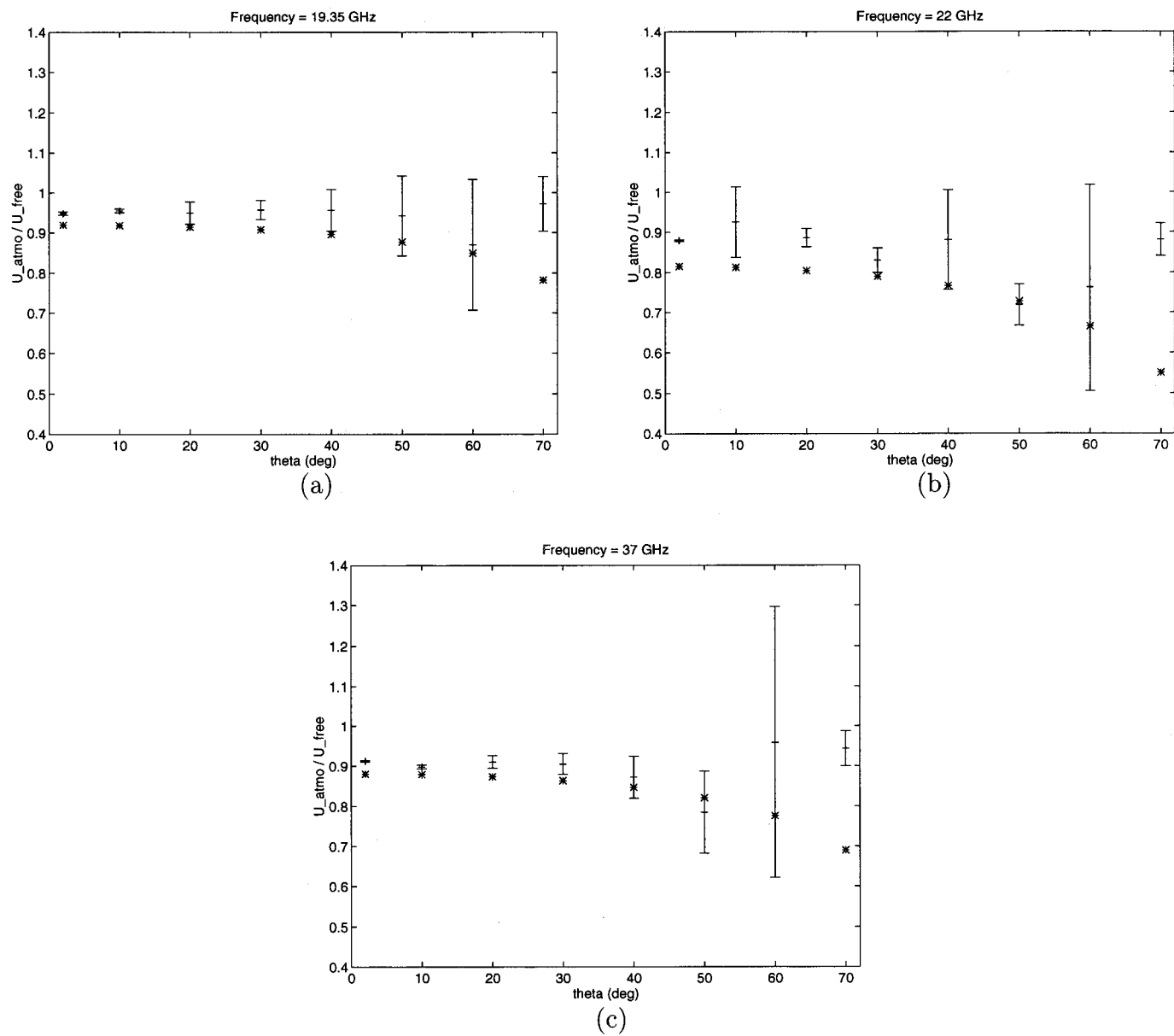Yeang, Yueh, Ding, and Kong, Figure 7

US Standard Atmosphere

(a)

Latitude 15 deg

(b)

Latitude 60 deg

(c)
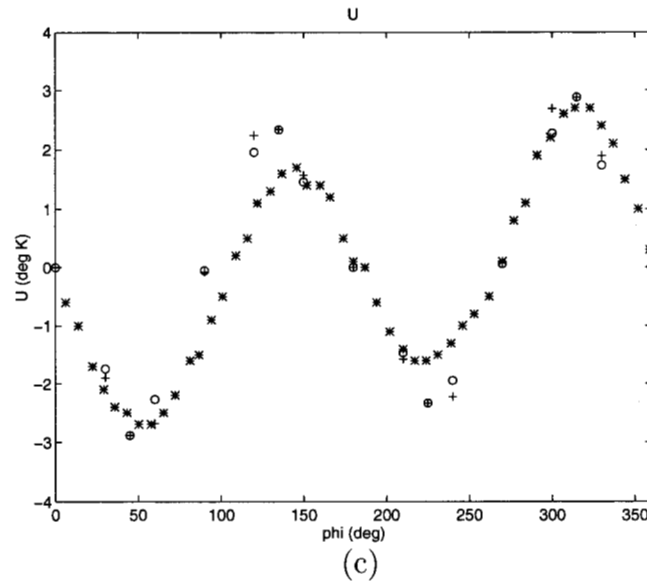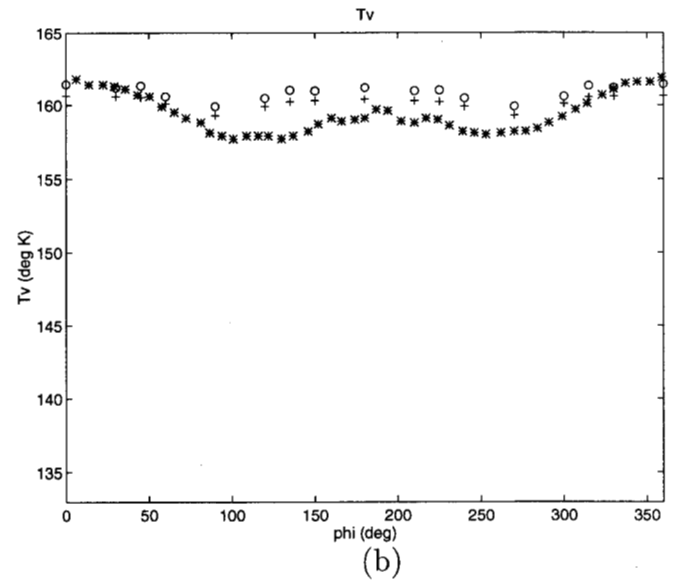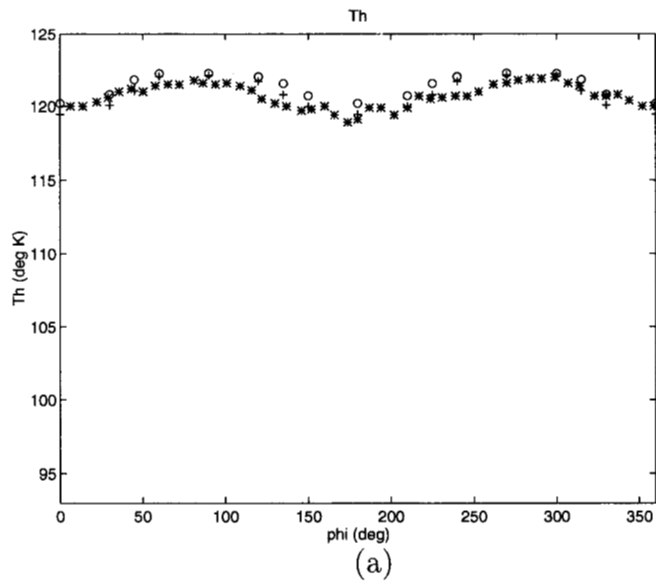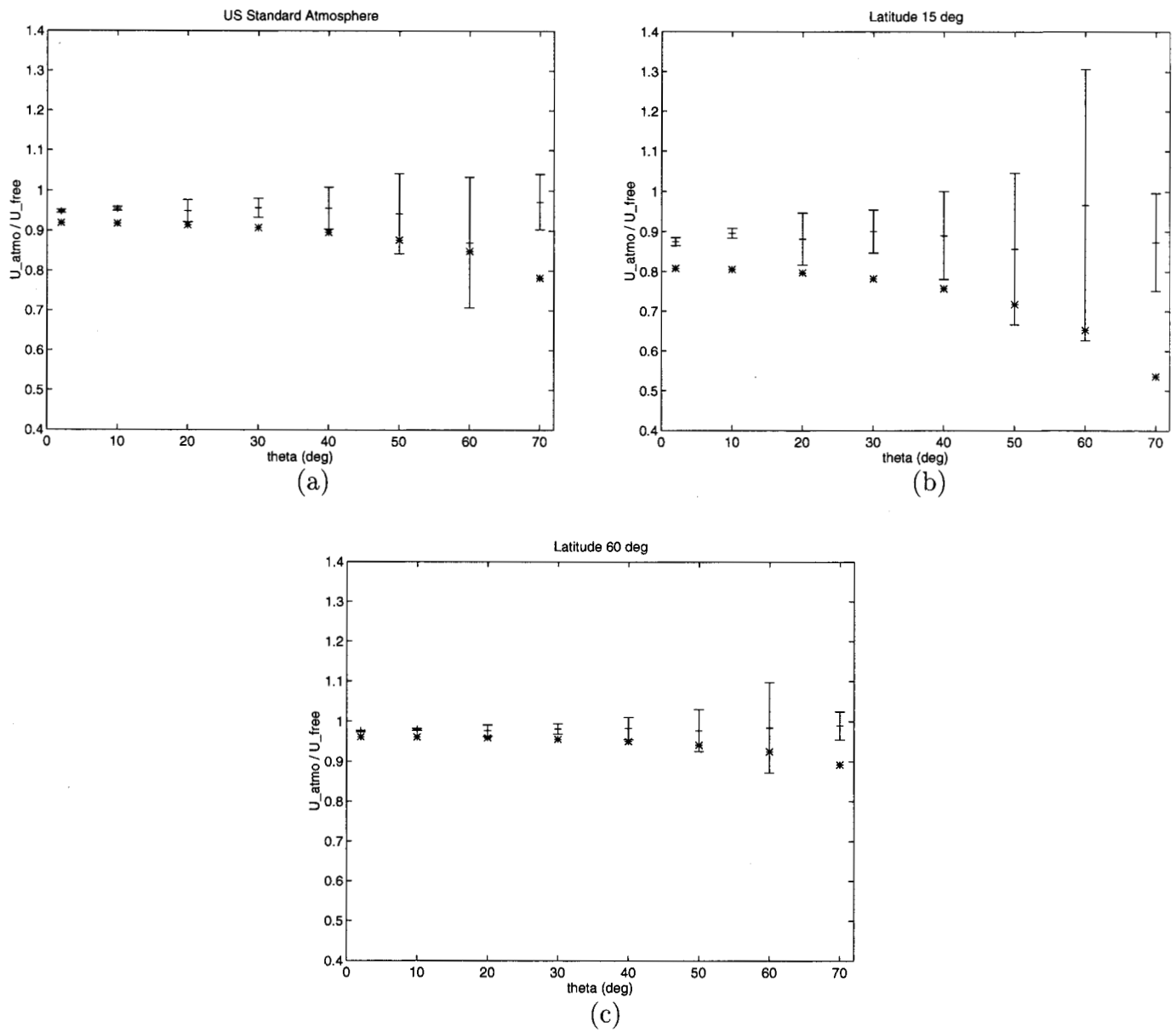
Yeang, Yueh, Ding, and Kong, Figure 8
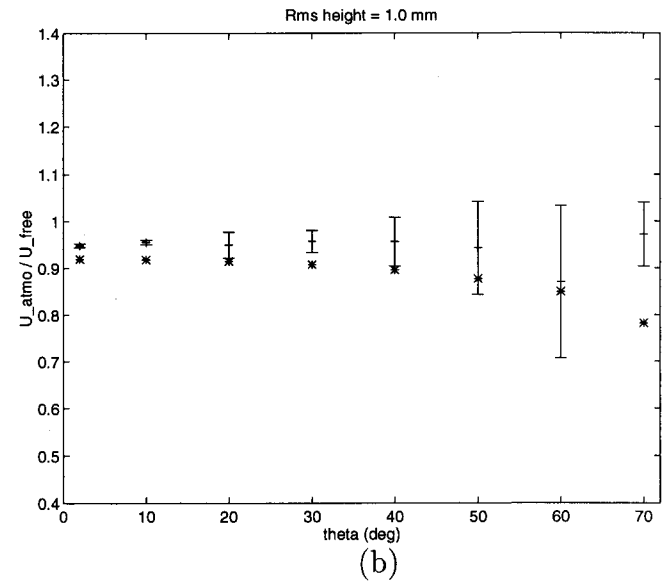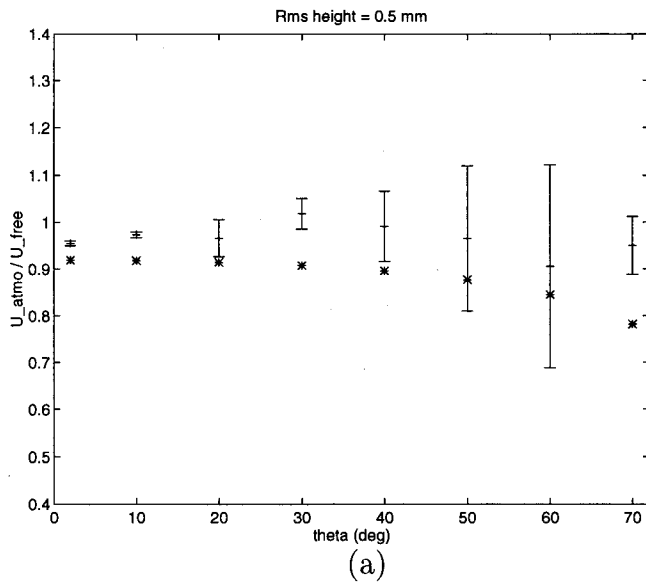
Yeang, Yueh, Ding, and Kong, Figure 9

Yeang, Yueh, Ding, and Kong, Figure 10